Electronic properties of BiTeX (X =Cl, Br, and I) through generalized tight-binding models: Orthogonal and nonorthogonal perspectives

S. Ganjehie[*] and S. Hessami Pilehrood[†]
Faculty of Physics, Shahrood University of Technology, Shahrud, Iran

S. A. Ketabi[‡]
School of Physics, Damghan University, Dāmghān, Iran

M. Nakhaee[§]
Department of Physics, Humboldt-Universität zu Berlin, Berlin, Germany

(Received 29 December 2023; revised 4 April 2024; accepted 17 April 2024; published 10 May 2024)

In this study, we employ a generalized tight-binding (TB) framework to explore the electronic characteristics of BiTeX (X = Cl, Br, and I) compounds. Our methodology relies on Slater-Koster integrals (SK) and the linear combination of atomic orbitals (LCAO) approach as the basis for our investigation. By refining generalized TB models through first-principles calculations, we establish an efficient and accurate quantum mechanical technique for predicting the electronic properties of halogenated bismuth telluride. Our research delves into various models that provide unique insights into the electronic behavior of BiTeX. Within an orthogonal TB model, the contributions from s and p orbitals define the band gap, making it suitable for analyzing low-energy phenomena near the Γ point. Furthermore, this model extends to incorporate the interplay between d and p orbitals, resulting in a more comprehensive depiction of the band structure. Conversely, a nonorthogonal TB model emphasizes the contributions of s and p orbitals, revealing intricate details of the electronic structure, albeit with potential computational complexities. Remarkably, this model demonstrates excellent agreement with first-principles calculations. Collectively, these models unveil the nuanced electronic nature of BiTeX, furnishing adaptable computational tools for materials science and quantum device applications.

DOI: 10.1103/PhysRevB.109.195138

I. INTRODUCTION

Numerous studies have extensively investigated the electronic and optical properties of both bulk and layered semiconductor structures. However, a recent emergence of a novel category of bulk semiconducting materials, exemplified by the bismuth tellurohalides BiTeX (where X = Cl, Br, or I), has sparked considerable interest in the field. These materials feature a wide band gap and host bulk and surface states characterized by significant spin-orbit (SO) splitting. Their noncentrosymmetric crystal structure, stemming from the absence of inversion symmetry, facilitates a distinctive lifting of the Kramers degeneracy attributed to the SO interaction. Consequently, both the valence and conduction band states exhibit discernible energy and momentum splittings [1]. Furthermore, angle-resolved photoemission spectroscopy (ARPES) has demonstrated that the loss of inversion symmetry in BiTeX results in the appearance of spin-orbit coupling (SOC) [2,3], which removes spin degeneracy and gives rise to various innovative phenomena such as Rashba spin splitting and Hall effects [4–6]. The crystal structure of BiTeX features a triple layer with X-Bi-Te stacking. In this structure, a central Bi layer is sandwiched between a Te layer and a halide layer [7]. These triple layers are bounded by weak van der Waals interactions. The crystal structure of BiTeX is categorized under space group P63mc for X = Cl, and P3m1 for X = Br and I [8]. Density functional theory (DFT) studies on BiTeX have offered valuable insights into its electronic structure and other significant properties. The robust SO interaction has notably influenced the electronic properties of BiTeBr and BiTeI, investigated through DFT methods [9]. Additionally, DFT analysis explored the electronic behavior of BiTeX under electric fields and mechanical stress, resulting in noteworthy changes in the structural band gap [10]. Extensive research has focused on elucidating the mechanical, optical, and thermoelectric characteristics of BiTeX [11], contributing to a deeper understanding of its intrinsic features and potential applications. While first-principles calculations are a common tool for material prognosis, their effectiveness is limited by computational requirements and cell sizes. Thus, there is a growing need to explore alternative methodologies that enable more complex computations. TB schemes, among other quantum methods, have been effectively utilized over the past two decades to examine electronic structures in various systems [12–14]. An example of utilizing the TB method involves the research conducted by Jones *et al.* in 2009. Their study determined the TB parameters by aligning energy-band values derived from highly precise first-principles DFT calculations [15]. Also in 2016 Ortenzi *et al.* compared a TB model based on the SK formalism with DFT and found a good agreement for the overall band structure [16].

[*]S.Ganjehie@shahroodut.ac.ir
[†]hessami@shahroodut.ac.ir
[‡]saketabi@du.ac.ir
[§]mohammad.nakhaee@physik.hu-berlin.de

The aim of our study is to leverage a generalized TB model using the TBStudio software [17], employing a simplified LCAO approach to calculate the electronic structure of BiTe*X* (with *X*=Cl, Br, and I). TBStudio serves as a quantum technical software package specifically designed for constructing TB models for nanoscale materials. In our investigation, we have delved into the electronic structure of BiTe*X* and compare our findings with those derived from DFT calculations. Section II outlines the model and computational techniques, followed by Sec. III, which presents results and discussions, culminating in Sec. IV with conclusions.

II. MODEL AND THE COMPUTATIONAL SCHEME

The TB model is a significant method used to calculate the band structure of solids. It is particularly useful in analyzing transport properties. The TB method is based on the assumption that the wave function of an electron in a crystal can be approximated as a LCAO localized on individual atoms. The electronic structure is described by a set of basis functions, usually atomic orbitals, which are then combined to form a complete set of wave functions. These basis functions can be either orthogonal functions or nonorthogonal functions. Orthogonal basis functions are those that are mutually perpendicular to each other. In the context of the TB method, this means that the overlap between different atomic orbitals is negligible. On the other hand, nonorthogonal basis functions are not mutually perpendicular, meaning that there is a significant overlap between different atomic orbitals.

The TB Hamiltonian's matrix elements are generated by coupling the orbitals located on atomic sites that are in close proximity to each other. These matrix elements offer an explanation for the hopping of electrons from one lattice site to another. The hopping amplitudes can be determined by constructing a TB model and replicating the band energies calculated through the first principles. The LCAO [18] is a highly effective, efficient, and easily implementable technique for calculating the band structure of materials. In this method, the molecular orbitals or band structure are constructed by combining the wave functions of individual atomic orbitals located on the constituent atoms. The main advantage of LCAO is that it can be applied to nonperiodic systems, which is a critical feature in many applications. Additionally, the LCAO method is often preferred for systems with a large number of atoms, as it provides cost and time savings. Therefore, the combination of LCAO and Green's function theory is a powerful tool for calculating electronic properties, especially for nonperiodic systems and systems with a large number of atoms.

The aim of the current study is to construct a generalized TB model based on the TBStudio software using a simplified LCAO approach for the calculation of the electronic structure of BiTe*X* (with *X*=Cl, Br, and I). Starting from the simplified LCAO method in combination with first-principles calculations (such as OpenMX or VASP packages), one can construct a TB model in the two-center approximation. By employing the SK technique, the system's TB Hamiltonian can be computed, and use a nonlinear fitting algorithm to find the best entries for both Hamiltonian and overlap matrices to reproduce the first-principles data. One can obtain expressions for the Hamiltonian and overlap matrix elements between different orbitals (s, p, and d orbitals with or without SOC) for the different atoms and present the SK coefficients in an orthogonal or nonorthogonal basis set. We have employed the SK approach and fitted the energy dispersion based on values derived from DFT. This technique enables us to derive expressions for the Hamiltonian and overlap matrix elements between distinct orbitals.

In principle, there exist an infinite number of atoms, each having an infinite number of orbitals, which can be used to explain the electronic structure of various crystal structures. By utilizing the LCAO technique, it becomes possible to limit the system under consideration to a finite number of atoms and a finite number of orbitals per atom. Moreover, this method enables the description of a system as a collection of noninteracting single particles. Slater and Koster [19] introduced integrals and demonstrated how to utilize SK to recreate data from first principles. In a number of systems, the SK method has been successful in creating TB Hamiltonians. In this work, the independent parameters for both the Hamiltonian and the overlap matrices are determined using the Levenberg-Marquardt approach to achieve an acceptable match with the first-principles data. The following equation presents the SK integrals of Hamiltonian and overlap matrix elements:

$$h_{ll'}^{mm'}(\vec{r}) = \left\langle \varphi_l^m(\vec{x}+\vec{r}) \middle| H(\vec{x}+\vec{r}) \middle| \varphi_{l'}^{m'}(\vec{x}) \right\rangle,$$
$$s_{ll'}^{mm'}(\vec{r}) = \left\langle \varphi_l^m(\vec{x}+\vec{r}) \middle| \varphi_{l'}^{m'}(\vec{x}) \right\rangle. \quad (1)$$

Here $\varphi_l^m(\mathbf{x})$ is the real spherical harmonic which can be explained in terms of the complex spherical harmonic Y_l^m. The vector $\vec{r}$ defines the bond between two atoms. Respectively, as a function of $\vec{r}$, $h_{ll'}^{mm'}(\vec{r})$ and $s_{ll'}^{mm'}(\vec{r})$ represent the elements of the overlap and Hamiltonian matrix that are defined in between the orbits of two distinct atoms. The SK method has proven to be effective in constructing TB Hamiltonians

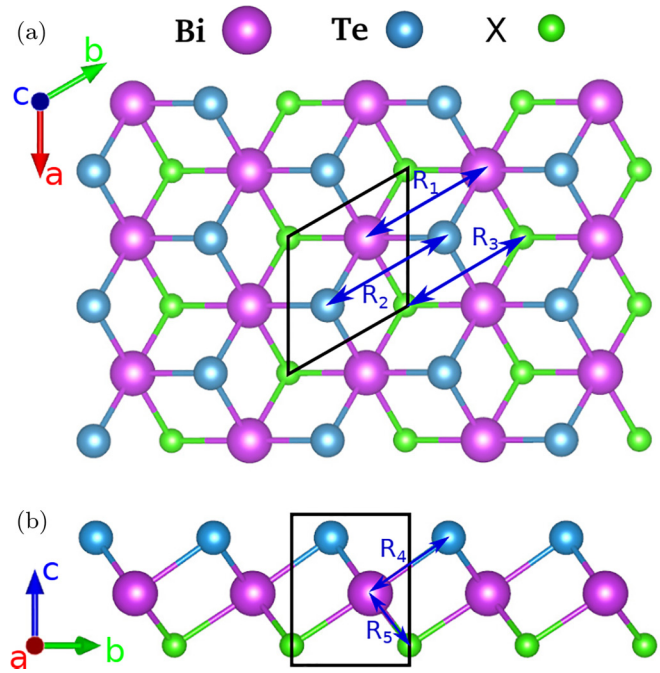

FIG. 1. (a) Top and (b) side view of the structure of BiTe*X*. The black box indicates the unit cell. The atoms that are used to build the TB model are depicted by the lattice vectors **a**, **b**, and **c**.

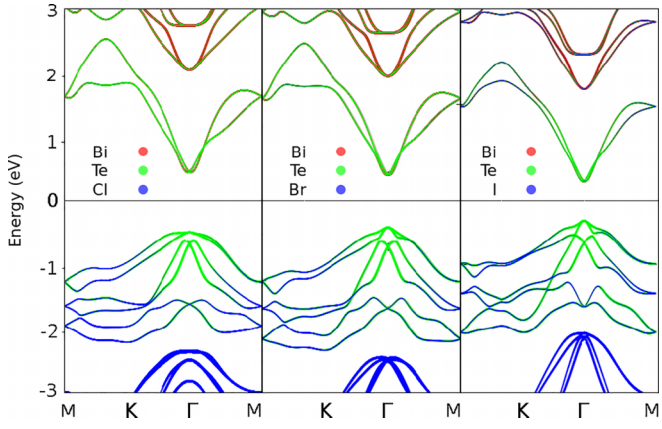

FIG. 2. The band structures of BiTeX (X = Cl, Br and I) which illustrate the contribution of Bi (red), Te (green), and X (blue) atoms.

for a variety of systems [20,21]. The SK integrals are key parameters in our generalized TB models that describe the hopping of electrons between atomic orbitals. These integrals capture the overlap and interactions between neighboring atoms and are crucial in determining the electronic structure of the material. To construct a TB model, we have first identified all SK integrals of the optimized structure in three sections. We then have used the final SK parameters, on-site energies, overlap parameters, and SOC values to construct the TB Hamiltonian. We have used the OpenMX software [22] to extract band structures from first-principles calculations and carry out computations on electronic properties and atomic structure relaxations in order to obtain insight into both the structure and the electronic properties of BiTeX. The Monkhorst-Pack mesh was used to evaluate numerical integrations within the Brillouin zone ($15 \times 15 \times 1$). We have employed a PBE functional [23,24] with a cutoff energy of 400 eV for the plane-wave basis and the generalized gradient approximation (GGA) for the exchange correlation energy in our calculations. The optimized structure of BiTeX is shown in Fig. 1, where the black box denotes the unit cell and the vectors $\mathbf{R}_i$ denote the atoms that must be included in the TB model due to their close proximity to one another.

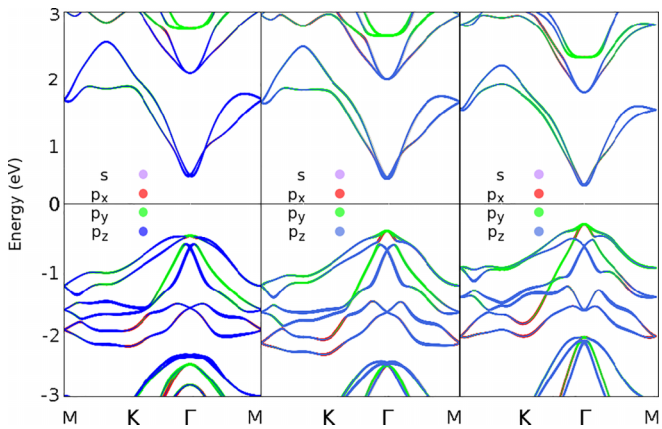

FIG. 3. The band structure of BiTeCl (left side), BiTeBr (center), and BiTeI (right side). The orbital contribution of atoms is denoted by s (pink), p_x (red), p_y (green), and p_z (blue) in band structure formation.

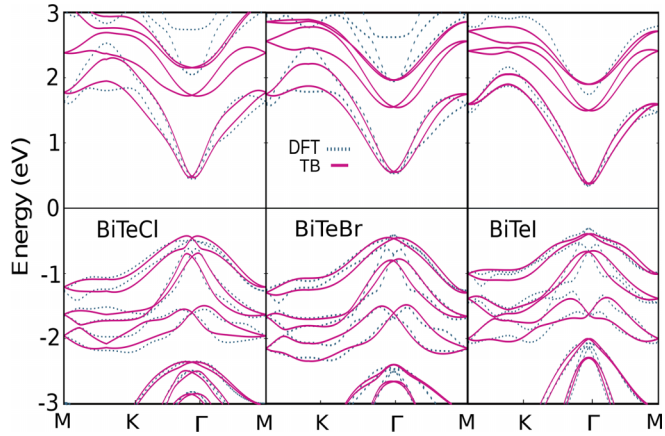

FIG. 4. The band structures of BiTeX calculated based on the orthogonal TB model using s and p orbital contributions with the SK parameters presented in Table I which are compared with the results of the DFT calculations.

III. ATOMIC SPIN-ORBIT COUPLING

Structures comprising heavy atoms exhibit a significant SO effect [25]. SOC is a fundamental mechanism that underlies the emergence of spin polarization in electronic states within solid materials. The SOC represents the interaction between the spin of a particle and its orbital motion. Experimentally, it has been observed that this particular occurrence manifests as a division of spectral lines [26–28]. The TB model can incorporate the atomic SO interaction in various ways, including

$$\hat{H}_{SO} = \frac{1}{2(m_e c)^2}(\nabla \mathbf{V} \times \mathbf{P}).\mathbf{S}, \tag{2}$$

where $\mathbf{P} = (\hbar/i)\nabla$ represents the electron momentum operator, while $\mathbf{S} = (\hbar/2)\boldsymbol{\sigma}$ denotes the electron spin operator. The components of the $\boldsymbol{\sigma}$ operators are specifically defined as the Pauli matrices and $\hbar$ is Planck's constant [29]. m_e represents the mass of a free electron and c is the speed of light. The potential gradient $\nabla \mathbf{V}$ depends on the atomic number Z. SO interactions can be exactly represented by a local atomic contribution of the form

$$\hat{H}_{SO} = \sum_i \sum_\nu \hat{P}_{i,\nu} \lambda_\nu \mathbf{L}_i.\mathbf{S}_i, \tag{3}$$

where S_i is the spin operator at site i, $\hat{P}_{i,\nu}$ is the projection operator for angular momentum ν at site i, and λ_ν is the SOC constant for angular momentum [12]. By calculating the operator $\mathrm{L} \otimes \mathrm{S}$, additional terms in the Hamiltonian can be identified, and the angular momentum and spin operators can be expressed as follows:

$$\vec{L} = (\mathbf{L}_x, \mathbf{L}_y, \mathbf{L}_z), \tag{4}$$

$$\vec{S} = (\mathbf{S}_x, \mathbf{S}_y, \mathbf{S}_z). \tag{5}$$

IV. RESULTS AND DISCUSSION

To illustrate the electronic band structures of BiTeX, the atomic and orbital contributions are delineated in detail in Figs. 2 and 3. These figures show the distribution of p_z, p_y, p_x, and s orbitals through blue, green, red, and pink curves,

TABLE I. The SK parameters, onsite energies, and SOC in the orthogonal TB model for BiTeX using *s* and *p* orbitals.

Bond		BiTeCl					BiTeBr					BiTeI				
Bond type	**R**	$ss\sigma$	$sp\sigma$	$pp\sigma$	$pp\pi$	$ss\sigma$	$sp\sigma$	$pp\sigma$	$pp\pi$	$ss\sigma$	$sp\sigma$	$pp\sigma$	$pp\pi$			
Bi-Bi	$\mathbf{R}_1$	−0.020	0.161	0.472	−0.292	−0.155	−0.333	0.015	−0.193	−0.005	−0.025	0.252	−0.186			
Te-Te	$\mathbf{R}_2$	0.009	−0.306	0.244	0.055	−0.178	−0.464	2.041	0.028	0.085	−0.349	0.265	0.075			
X-X	$\mathbf{R}_3$	0.000	−0.193	0.044	0.005	0.155	−0.150	0.108	0.011	−0.088	−0.203	0.001	0.038			
Bi-Te	$\mathbf{R}_4$	−0.734	1.768	1.661	−0.508	−0.588	−1.088	4.085	−1.263	−0.611	1.097	1.685	−0.506			
Bi-X	$\mathbf{R}_5$	−0.387	−0.243	−1.860	0.115	0.047	0.559	−1.281	0.183	−0.364	−0.654	−2.038	0.152			
Atom		s	p_x	p_y	p_z	α^p_{so}	s	p_x	p_y	p_z	α^p_{so}	s	p_x	p_y	p_z	α^p_{so}
Bi		−9.086	0.441	0.274	−0.344	−0.610	−4.557	−0.903	−2.050	−1.787	−1.552	−10.161	0.027	−0.038	−0.979	−0.695
Te		−9.353	−1.497	−2.272	−2.329	−0.670	−2.522	−2.675	−3.871	0.559	−2.911	−9.408	−1.705	−1.995	−2.290	−0.849
X		−14.340	−1.876	−1.543	−1.231	−0.035	−3.370	−2.297	−1.319	−4.253	−0.052	−13.141	−0.916	−0.795	−1.369	−0.150

respectively. Within the energy range of −6 eV to −15 eV, the electronic band structures are primarily influenced by the *s* orbitals, exhibiting significant separation from the electronic bands below them, forming a sizable band gap. The region spanning from −6 eV to 0 eV below the band gap is identified as the valence band, while the area above the band gap is referred to as the conduction band. Previous studies on BiTe*X* crystals [30] indicate that the conduction bands primarily consist of *p* orbitals from Bi and Te atoms, while the valence band is predominantly composed of *p* orbitals from halogen atoms. It is worth noting that Bi orbital states are distant from the Fermi level, whereas Te-*p* and *X*-*p* orbital states play a crucial role in occupying electronic states near the Fermi level. The increase in electronegativity of element *X* from I to Cl results in a noticeable downward shift of its lower band energies, highlighting the significant contribution of *X* atoms to the valence band. Moreover, in all examined scenarios, the minimum conduction band and maximum valence band are positioned at the Γ high symmetry point.

V. ORTHOGONAL TB MODEL FOR BiTeX USING *s* AND *p* ORBITALS

The orthogonal TB model tailored for BiTeX focuses specifically on *s* and *p* orbitals to capture the intricate electronic structure of this compound. As depicted in Fig. 3, the inclusion of *p* orbitals in reconstructing the band structure proved to be indispensable. Throughout the fitting process, we find that accounting for the interaction between *s* and *p* orbitals is essential for achieving accurate representation of the material's electronic behavior. Neglecting or underestimating this interaction resulted in significant discrepancies between the model predictions and the actual electronic properties observed in the material. This customized TB approach, integrating both *s* and *p* orbitals, offers invaluable insights into the fundamental electronic characteristics of BiTe*X*, while the orthogonality constraint simplifies computational complexity. The result related to this method is presented in Fig. 4, and the on-site energies and SK parameters for the Hamiltonian and overlap matrix are provided in Table I. This model effectively identifies the bands around the Fermi level, with a primary focus on accurate fitting for the energy gap. Notably, the reduction in matrix size enhances computational efficiency without undermining accuracy, showcasing commendable alignment with first-principles calculations. Thus, it stands as a viable choice for computations primarily centered on low-energy considerations around the Γ point. In Fig. 4, the Fermi energy level is set as the reference at zero. Across all three BiTe*X* structures depicted, similarities in their distinctive characteristics were noted. However, upon incorporating SOC into the computational analysis, a notable increase in the band count becomes apparent. Furthermore, the valence band maximum and conduction band minimum, originally situated at the Γ -point, exhibit a noticeable separation, resulting in a reduction in the magnitude of the band gap. The band structure of BiTe*X* showcases a pronounced Rashba effect and robust SO interactions, leading to significant spin splitting for electrons near the conduction band minimum and holes near the valence band maximum [31]. The experimental finding aligns seamlessly with the aforementioned factors [32–35].

VI. ORTHOGONAL TB MODEL FOR BiTeX USING *s*, *p*, AND *d* ORBITALS

Here, we present the results of an orthogonal TB model for BiTe*X*. This model involves parametrization using *s*, *p* and *d* orbitals to describe the electronic structure of the BiTe*X* compound. As depicted in Fig. 3, the primary focus lies on

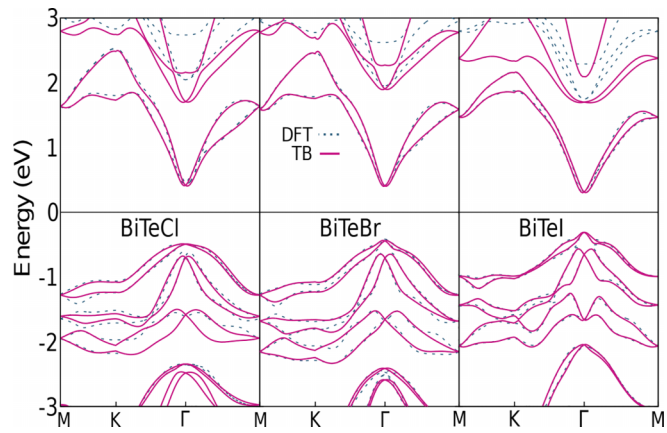

FIG. 5. The band structures of BiTe*X* calculated based on the orthogonal TB model using *s*, *p*, and *d* orbital contributions with the SK parameters presented in Tables II, III, and IV which are compared with the results of the DFT calculations.

TABLE II. The SK parameters, onsite energies, and SOC in the orthogonal TB model for BiTeCl using s, p, and d orbitals.

Bond type	**R**	$ss\sigma$	$sp\sigma$	$pp\sigma$	$pp\pi$	$sd\sigma$	$pd\sigma$	$pd\pi$	$dd\sigma$	$dd\pi$	$dd\delta$
Bi-Bi	$\mathbf{R}_1$	−0.554	−0.388	−0.046	0.0632	−1.187	1.578	−0.097	−2.149	−3.204	0.819
Te-Te	$\mathbf{R}_2$	−0.296	−0.517	−0.050	0.039	−3.281	−1.184	−0.056	9.684	2.768	8.595
X-X	$\mathbf{R}_3$	0.046	0.206	−0.026	−0.037	−0.795	2.556	−0.116	21.416	35.258	9.844
Bi-Te	$\mathbf{R}_4$	0.998	1.265	2.701	−0.635	2.372	2.102	−7.675	68.062	−8.153	−2.636
Bi-X	$\mathbf{R}_4$	−2.650	−0.342	−1.014	0.128	−1.939	1.964	1.415	−34.207	7.328	−16.240
Atom	s	p_x	p_y	p_z	d_{xy}	d_{yz}	d_{xz}	$d_{x^2-y^2}$	$d_{r^2-z^2}$	α^p_{so}	α^d_{so}
Bi	−5.427	−0.186	0.401	0.075	185.887	198.899	164.785	186.646	199.890	−0.531	0.000
Te	−6.573	0.591	0.762	−0.672	187.165	138.506	164.708	194.045	174.293	−1.650	0.000
X	−12.182	−2.352	−1.865	−1.872	191.376	187.900	191.223	198.001	187.099	−0.067	0.000

TABLE III. The SK parameters, onsite energies, and SOC in the orthogonal TB model for BiTeBr using s, p, and d orbitals.

Bond type	**R**	$ss\sigma$	$sp\sigma$	$pp\sigma$	$pp\pi$	$sd\sigma$	$pd\sigma$	$pd\pi$	$dd\sigma$	$dd\pi$	$dd\delta$
Bi-Bi	$\mathbf{R}_1$	−0.593	−0.401	−0.072	0.116	−1.344	2.275	−0.264	−14.941	−2.306	4.060
Te-Te	$\mathbf{R}_2$	0.042	−0.430	−0.015	0.038	−2.827	−1.650	0.661	2.139	−3.833	9.629
X-X	$\mathbf{R}_3$	0.088	0.334	−0.025	−0.031	−6.578	2.805	0.115	29.289	31.630	−1.455
Bi-Te	$\mathbf{R}_4$	0.965	1.259	2.782	−0.674	1.801	1.877	−7.529	59.891	−10.358	−13.163
Bi-X	$\mathbf{R}_4$	−2.669	−0.329	−1.178	0.154	−3.955	1.513	1.128	−51.775	24.422	−23.522
Atom	s	p_x	p_y	p_z	d_{xy}	d_{yz}	d_{xz}	$d_{x^2-y^2}$	$d_{r^2-z^2}$	α^p_{so}	α^d_{so}
Bi	−5.642	−0.207	0.148	−0.171	199.365	199.258	144.845	198.665	192.745	−0.644	0.000
Te	−6.526	0.520	1.000	−0.372	156.236	138.630	184.383	199.453	151.535	−1.720	0.000
X	−12.310	−2.391	−1.862	−2.064	164.990	93.131	180.744	182.055	198.473	−0.130	0.000

TABLE IV. The SK parameters, onsite energies, and SOC in the orthogonal TB model for BiTeI using s, p, and d orbitals.

Bond type	**R**	$ss\sigma$	$sp\sigma$	$pp\sigma$	$pp\pi$	$sd\sigma$	$pd\sigma$	$pd\pi$	$dd\sigma$	$dd\pi$	$dd\delta$
Bi-Bi	$\mathbf{R}_1$	−0.498	−0.508	−0.137	0.183	−3.507	3.551	−0.011	1.326	−2.058	−4.222
Te-Te	$\mathbf{R}_2$	0.383	−0.368	0.203	−0.025	−4.252	−1.965	0.578	8.342	2.468	−9.525
X-X	$\mathbf{R}_3$	0.693	0.177	0.129	−0.046	7.028	2.606	−0.707	21.783	10.835	28.877
Bi-Te	$\mathbf{R}_4$	0.432	1.508	2.352	−0.567	0.116	−3.279	−6.510	56.618	−7.319	−12.034
Bi-X	$\mathbf{R}_4$	−1.979	−0.583	−1.247	0.222	−2.322	0.030	1.252	−58.913	22.654	−9.841
Atom	s	p_x	p_y	p_z	d_{xy}	d_{yz}	d_{xz}	$d_{x^2-y^2}$	$d_{r^2-z^2}$	α^p_{so}	α^d_{so}
Bi	−5.878	−0.197	0.230	−0.557	169.464	160.931	152.491	185.674	173.379	−0.706	0.000
Te	−7.140	0.612	0.747	0.842	174.291	111.170	138.429	183.291	199.904	−1.345	0.000
X	−12.678	−2.143	−1.947	−2.117	189.181	183.396	107.944	135.123	164.357	−0.266	0.000

TABLE V. The SK parameters, onsite energies, SOC, and overlap parameters in the nonorthogonal TB model for BiTeCl using s and p orbitals.

Bond		Hamiltonian				Overlap matrix			
Bond type	**R**	$ss\sigma$	$sp\sigma$	$pp\sigma$	$pp\pi$	$ss\sigma$	$sp\sigma$	$pp\sigma$	$pp\pi$
Bi-Bi	$\mathbf{R}_1$	−0.795	0.439	0.830	−0.206	0.060	−0.036	−0.066	0.052
Te-Te	$\mathbf{R}_2$	−0.960	−0.334	0.156	−0.007	0.075	−0.018	−0.101	0.013
X-X	$\mathbf{R}_3$	−0.413	−0.165	−0.109	−0.232	0.029	0.001	0.074	0.112
Bi-Te	$\mathbf{R}_4$	−0.754	1.634	1.521	−0.946	0.100	−0.123	−0.063	−0.071
Bi-X	$\mathbf{R}_5$	−0.708	−0.473	0.667	0.103	0.067	0.098	0.355	0.069
Te-X	$\mathbf{R}_6$	−4.811	−0.171	0.667	−0.340	0.337	−0.057	−0.298	0.073
Atom	s	p_x	p_y	p_z	α^p_{so}				
Bi	−10.760	0.638	0.898	0.496	0.407				
Te	−10.602	−1.210	−1.072	−1.754	−0.652				
X	−13.951	−2.371	−1.998	−1.975	0.052				

TABLE VI. The SK parameters, onsite energies, SOC, and overlap parameters in the nonorthogonal TB model for BiTeBr using s and p orbitals.

Bond		Hamiltonian				Overlap matrix			
Bond type	**R**	$ss\sigma$	$sp\sigma$	$pp\sigma$	$pp\pi$	$ss\sigma$	$sp\sigma$	$pp\sigma$	$pp\pi$
Bi-Bi	$\mathbf{R}_1$	−0.680	−0.439	0.350	−0.362	0.030	0.006	−0.139	0.074
Te-Te	$\mathbf{R}_2$	0.349	−0.759	0.370	−0.016	0.003	0.060	−0.017	−0.035
X-X	$\mathbf{R}_3$	−0.717	0.112	0.621	0.139	0.112	−0.026	−0.021	−0.037
Bi-Te	$\mathbf{R}_4$	−0.046	1.077	1.770	−1.065	−0.002	−0.104	−0.313	0.009
Bi-X	$\mathbf{R}_5$	−0.642	2.699	0.776	0.344	0.118	−0.122	0.225	−0.058
Te-X	$\mathbf{R}_6$	1.959	1.093	0.372	−0.382	−0.241	0.032	−0.111	0.035
Atom	s	p_x	p_y	p_z	α^p_{so}				
Bi	−10.656	0.077	2.042	−2.839	0.171				
Te	−8.678	−1.113	−1.974	−1.338	−0.607				
X	−11.672	−2.851	−3.445	−3.948	−0.162				

the p_x, p_y, and p_z orbitals, representing the p orbitals, as the key orbitals to be utilized in the model. Meanwhile, the d orbitals are treated as free parameters that indirectly influence the model through their coupling with the p orbitals. This coupling introduces an additional layer of complexity and flexibility to the model, allowing for the consideration of the d orbitals' contributions to electronic interactions. While the d orbitals might not be explicitly included in the fitting process, their effects on the p orbitals through their coupling interactions are taken into account, providing a more comprehensive representation of the material's electronic behavior within the TB method. Additionally, the significance of the SOC for d orbitals in BiTeX structures is minimal. The orthogonal s-p-d model aims to capture the interactions between p and d orbitals within the material by considering the interaction integrals between these orbitals. As demonstrated in Fig. 5 and Tables II, III, and IV, by incorporating s, p, and d orbitals, the model accounts for the varying spatial distributions and energies of electrons in the system, enabling a more detailed description of the band structures, suitable for investigating more accurate electronic properties, densities of states, and other relevant characteristics specific to the BiTeX compound. The $\mathbf{S} = I$ constraint ensures that the basis set formed by these orbitals remains mathematically orthogonal, and the calculations are straightforward, aiding in balancing computational efficiency and accuracy while providing a comprehensive representation of the material's electronic behavior.

VII. NONORTHOGONAL TB MODEL FOR BiTeX USING s AND p ORBITALS

The alternative model for BiTeX is a nonorthogonal TB model that utilizes s and p orbitals to capture the intricate electronic structure of this compound. Unlike traditional orthogonal models, this approach allows for a more detailed description of the material's electronic properties, accommodating nonorthogonality between the orbitals. However, this approach might entail increased computational complexity due to the inclusion of nonorthogonal terms, yet it promises a richer understanding of the material's electronic structure, offering valuable insights for various technological applications. The results are presented in Fig. 6, and the on-site energies and SK parameters for the Hamiltonian and overlap matrix are listed in Tables V, VI, and VII. The nonorthogonal TB model demonstrates exceptional agreement with first-principle calculations, offering heightened computational efficiency. Notably, it stands out as a robust option capable of computations across the entire Brillouin zone, not restricting

TABLE VII. The SK parameters, onsite energies, SOC, and overlap parameters in the nonorthogonal TB model for BiTeI using s and p orbitals.

Bond		Hamiltonian				Overlap matrix			
Bond type	**R**	$ss\sigma$	$sp\sigma$	$pp\sigma$	$pp\pi$	$ss\sigma$	$sp\sigma$	$pp\sigma$	$pp\pi$
Bi-Bi	$\mathbf{R}_1$	−0.208	−0.105	0.200	−0.172	−0.002	−0.020	−0.086	0.019
Te-Te	$\mathbf{R}_2$	0.226	−0.201	0.230	−0.142	−0.003	0.016	−0.070	0.017
X-X	$\mathbf{R}_3$	0.150	0.052	0.282	0.028	0.003	0.010	0.057	0.007
Bi-Te	$\mathbf{R}_4$	−0.105	0.700	1.721	−0.954	0.034	0.007	0.020	0.018
Bi-X	$\mathbf{R}_5$	0.681	1.776	1.787	−0.035	0.001	−0.005	−0.014	0.024
Te-X	$\mathbf{R}_6$	−0.032	1.063	−0.053	−0.202	−0.036	−0.004	0.097	0.048
Atom	s	p_x	p_y	p_z	α^p_{so}				
Bi	−9.991	0.428	0.911	−1.602	0.248				
Te	−8.984	−0.641	−1.438	−1.235	−0.527				
X	−11.544	−2.115	−2.116	−3.525	−0.233				

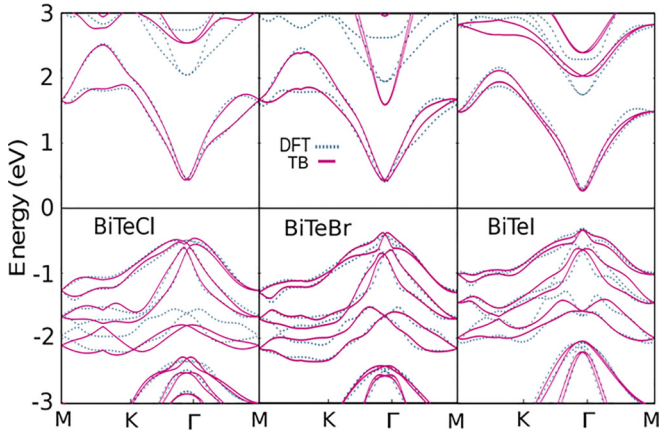

FIG. 6. The band structures of BiTeX calculated based on the nonorthogonal TB model using s and p orbital contributions with the SK parameters presented in Tables V, VI, and VII which are compared with the results of the DFT calculations.

analyses solely to the Γ point or low-energy regimes. Its capacity to span the entire Brillouin zone signifies its potential for comprehensive investigations of electronic properties throughout the material's structure, rendering it a strong candidate for diverse computational studies beyond localized and low-energy considerations.

VIII. CONCLUSIONS

In summary, we have examined the electronic structure of BiTeX (with X = Cl, Br, and I) using a generalized TB method, highlighting the role of different orbitals in shaping BiTeX's electronic properties. Each model presents distinct advantages, ranging from computational efficiency to comprehensive coverage across the Brillouin zone, catering to diverse computational requirements and offering insights into BiTeX's electronic behavior. We have introduced three specific TB models, each designed for particular purposes: orthogonal s-p, orthogonal s-p-d, and nonorthogonal s-p models. The orthogonal s-p TB model effectively captures BiTeX's electronic properties, emphasizing precise fitting for the gap energy. It aligns well with first-principles calculations and provides computational efficiency for low-energy considerations around the Γ point. In the orthogonal s-p-d model, the coupling interactions between d and p orbitals add complexity to the model, although SOC in BiTeX remains minimal. On the other hand, the nonorthogonal s-p model, relying on s and p orbitals, offers a more detailed representation of electronic properties despite potential computational complexity. This model exhibits excellent agreement with first-principles calculations and provides versatility for comprehensive computations across the entire Brillouin zone.

ACKNOWLEDGMENT

The authors acknowledge M. Shiranzaei for her useful discussion.

[1] L. Moreschini, G. Autes, A. Crepaldi, S. Moser, J. C. Johannsen, K. S. Kim, H. Berger, P. Bugnon, A. Magrez, J. Denlinger, and E. Rotenberg, J. Electron Spectrosc. Relat. Phenom. **201**, 115 (2015).
[2] I. Crassee, F. Borondics, M. K. Tran, G. Autès, A. Magrez, P. Bugnon, and A. Akrap, Phys. Rev. B **95**, 045201 (2017).
[3] J. Qu, X. Han, S. Sakamoto, C. J. Jia, J. Liu, H. Li, and J. A. Sobota, npj Quantum Mater. **8**, 13 (2023).
[4] K. Ishizaka, M. S. Bahramy, H. Murakawa, M. Sakano, T. Shimojima, T. Sonobe, K. Koizumi, S. Shin, H. Miyahara, A. Kimura, and K. Miyamoto, Nat. Mater. **10**, 521 (2011).
[5] A. Crepaldi, L. A. G. T. Moreschini, G. Autes, C. Tournier-Colletta, S. Moser, N. Virk, H. Berger, Ph. Bugnon, Y. J. Chang, K. Kern, and A. Bostwick, Phys. Rev. Lett. **109**, 096803 (2012).
[6] I. Y. Sklyadneva, R. Heid, K. P. Bohnen, V. Chis, V. A. Volodin, K. A. Kokh, O. E. Tereshchenko, P. M. Echenique, and E. V. Chulkov, Phys. Rev. B **86**, 094302 (2012).
[7] S. Schwalbe, R. Wirnata, R. Starke, Giulio A. H. Schober, and J. Kortus, Phys. Rev. B **94**, 205130 (2016).
[8] J. Kim, K. M. Rabe, and D. Vanderbilt, Phys. Rev. B **100**, 104115 (2019).
[9] V. A. Kulbachinskii, V. G. Kytin, A. A. Kudryashov, A. N. Kuznetsov, and A. V. Shevelkov, J. Solid State Chem. **193**, 154 (2012).
[10] A. Bafekry, S. Karbasizadeh, C. Stampfl, M. Faraji, D. M. Hoat, I. A. Sarsari, S. A. H. Feghhi, and M. Ghergherehchi, Phys. Chem. Chem. Phys. **23**, 15216 (2021).
[11] P. Chauhan, J. Singh, and A. Kumar, J. Phys. Chem. Solids **167**, 110758 (2022).
[12] F. Mangussi, M. Milićević, I. Sagnes, L. Le Gratiet, A. Harouri, A. Lemaître, J. Bloch, A. Amo, and G. Usaj, J. Phys.: Condens. Matter **32**, 315402 (2020).
[13] V. N. Popov and L. Henrard, Phys. Rev. B **70**, 115407 (2004).
[14] A. S. Martins and C. E. Fellows, Braz. J. Phys. **46**, 621 (2016).
[15] M. D. Jones and R. C. Albers, Phys. Rev. B **79**, 045107 (2009).
[16] L. Ortenzi, E. Cappelluti, and L. Pietronero, Phys. Rev. B **94**, 064507 (2016).
[17] M. Nakhaee, S. A. Ketabi, and F. M. Peeters, Comput. Phys. Commun. **254**, 107379 (2020).
[18] T. Clark and R. B. Koch, *Machine Learning: A Probabilistic Perspective* (Springer Science, Berlin, 2013).
[19] J. C. Slater and G. F. Koster, Phys. Rev. **94**, 1498 (1954).
[20] M. Nakhaee, S. A. Ketabi, and F. M. Peeters, Phys. Rev. B **97**, 125424 (2018).
[21] M. Nakhaee, S. A. Ketabi, and F. M. Peeters, Phys. Rev. B **98**, 115413 (2018).
[22] S. Boker, M. Neale, H. Maes, M. Wilde, M. Spiegel, T. Brick, J. Spies, R. Estabrook, S. Kenny, T. Bates, and P. Mehta, Psychometrika **76**, 306 (2011).
[23] J. P. Perdew, K. Burke, and M. Ernzerhof, Phys. Rev. Lett. **77**, 3865 (1996).
[24] A. D. Becke, Phys. Rev. A **38**, 3098 (1988).
[25] Y. Zhang, N. Yamaguchi, H. Sawahata, and F. Ishii, Appl. Phys. Express **16**, 053002 (2023).

[26] I. I. Klimovskikh, A. M. Shikin, M. M. Otrokov, A. Ernst, I. P. Rusinov, O. E. Tereshchenko, V. A. Golyashov, J. Sanchez-Barriga, A. Y. Varykhalov, O. Rader, K. A. Kokh, and E. V. Chulkov, Sci. Rep. **7**, 3353 (2017).

[27] G. Landolt, S. V. Eremeev, O. E. Tereshchenko, S. Muff, K. A. Kokh, J. Osterwalder, E. V. Chulkov, and J. H. Dil, Phys. Rev. B **91**, 081201(R) (2015).

[28] H. J. Noh, H. Koh, S. J. Oh, J. H. Park, H. D. Kim, J. D. Rameau, T. Valla, T. E. Kidd, P. D. Johnson, Y. Hu, and Q. Li, Europhys. Lett. **81**, 57006 (2008).

[29] M. Combescot, S. Y. Shiau, and V. Voliotis, Phys. Rev. B **99**, 245202 (2019).

[30] M. J. Varjovi and E. Durgun, Phys. Rev. Mater. **5**, 104001 (2021).

[31] Z. Kovács-Krausz, A. M. Hoque, P. Makk, B. Szentpéteri, M. Kocsis, B. Fülöp, M. V. Yakushev, T. V. Kuznetsova, O. E. Tereshchenko, K. A. Kokh, and I. E. Lukács, Nano Lett. **20**, 4782 (2020).

[32] H. Maaß, H. Bentmann, C. Seibel, C. Tusche, S. V. Eremeev, T. R. Peixoto, O. E. Tereshchenko, K. A. Kokh, E. V. Chulkov, J. Kirschner, and F. Reinert, Nat. Commun. **7**, 11621 (2016).

[33] J. Z. Xin, C. G. Fu, W. J. Shi, G. W. Li, G. Auffermann, Y. P. Qi, T. J. Zhu, X. B. Zhao, and C. Felser, Rare Met. **37**, 274 (2018).

[34] A. Akrap, J. Teyssier, A. Magrez, P. Bugnon, H. Berger, A. B. Kuzmenko, and D. Van Der Marel, Phys. Rev. B **90**, 035201 (2014).

[35] G. Landolt, S. V. Eremeev, O. E. Tereshchenko, S. Muff, B. Slomski, K. A. Kokh, M. Kobayashi, T. Schmitt, V. N. Strocov, J. Osterwalder, and E. V. Chulkov, New J. Phys. **15**, 085022 (2013).